

See discussions, stats, and author profiles for this publication at: <https://www.researchgate.net/publication/256200111>

Self-Assembly in Mixtures of an Anionic and a Cationic Surfactant: A Comparison between Small-Angle Neutron Scattering and Cryo-Transmission Electron Microscopy

ARTICLE *in* **LANGMUIR** · AUGUST 2013

Impact Factor: 4.46 · DOI: 10.1021/la401884k · Source: PubMed

CITATIONS

7

READS

43

5 AUTHORS, INCLUDING:

[Magnus Bergstrom](#)

Uppsala University

62 PUBLICATIONS 1,566 CITATIONS

[SEE PROFILE](#)



[Sara Skoglund](#)

KTH Royal Institute of Technology

11 PUBLICATIONS 175 CITATIONS

[SEE PROFILE](#)



[Katarina Edwards](#)

Uppsala University

148 PUBLICATIONS 5,444 CITATIONS

[SEE PROFILE](#)



[Isabelle Grillo](#)

Institut Laue-Langevin

142 PUBLICATIONS 2,530 CITATIONS

[SEE PROFILE](#)

Self-Assembly in Mixtures of an Anionic and a Cationic Surfactant: A Comparison between Small-Angle Neutron Scattering and Cryo-Transmission Electron Microscopy

L. Magnus Bergström,^{*,†} Sara Skoglund,[†] Katarina Edwards,[‡] Jonny Eriksson,[‡] and Isabelle Grillo[§]

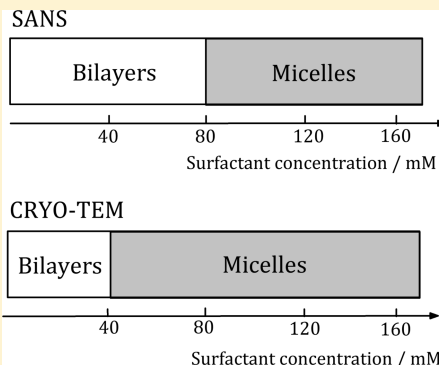
[†]Department of Chemistry, Surface, and Corrosion Science, School of Chemical Science and Engineering, KTH Royal Institute of Technology, SE-10044 Stockholm, Sweden

[‡]Department of Chemistry - BMC, Uppsala University, Box 579, SE-75123 Uppsala, Sweden

[§]Institut Laue Langevin, DS/LSS, 6 rue Jules Horowitz, BP156, 38042 Grenoble Cedex 9, France

S Supporting Information

ABSTRACT: The self-assembly in SOS-rich mixtures of the anionic surfactant sodium octyl sulfate (SOS) and the cationic surfactant hexadecyltrimethylammonium bromide (CTAB) has been investigated with the complementary techniques small-angle neutron scattering (SANS) and cryo-transmission electron microscopy (cryo-TEM). Both techniques confirm the simultaneous presence of open and closed bilayer structures in highly diluted samples as well as the existence of small globular and large elongated micelles at higher concentrations. However, the two techniques sometimes differ with respect to which type of aggregates is present in a particular sample. In particular, globular or wormlike micelles are sometimes observed with cryo-TEM in the vicinity of the micelle-to-bilayer transition, although only bilayers are present according to SANS and the samples appear bluish to the eye. A similar discrepancy has previously been reported but could not be satisfactorily rationalized. On the basis of our comparison between *in situ* (SANS) and *ex situ* (cryo-TEM) experimental techniques, we suggest that this discrepancy appears mainly as a result of the non-negligible amount of surfactant adsorbed at interfaces of the thin sample film created during the cryo-TEM specimen preparation. Moreover, from our detailed SANS data analysis, we are able to observe the unusually high amount of free surfactant monomers present in SOS-rich mixtures of SOS and CTAB, and the experimental results give excellent agreement with model calculations based on the Poisson–Boltzmann mean field theory. Our careful comparison between model calculations and experiments has enabled us to rationalize the dramatic microstructural transformations frequently observed upon simply diluting mixtures of an anionic and a cationic surfactant.



INTRODUCTION

Two or more surfactants may self-assemble in an aqueous solvent to form common aggregates, such as micelles and bilayers, in which the amphiphilic components are able to mix with one another. As a result, an additional degree of freedom in terms of surfactant composition in the self-assembled aggregates appears and may have a considerable impact on the structural properties of the aggregates. For instance, mixing a single-tailed surfactant, which forms micelles on its own, with a double-tailed surfactant or lipid, which forms bilayer structures on its own, may generate a continuous growth of micelles, and a subsequent transition to bilayers, upon tuning the surfactant composition.^{1–7} A similar sequence of different structures ranging from small globular micelles to larger bilayer structures may be observed as two oppositely charged surfactants are mixed in aqueous solutions.^{8–25}

The composition in mixed self-assembled aggregates has been found to strongly depend on total surfactant concentration in dilute solutions.²⁶ The effect is found to be particularly pronounced in mixtures of two surfactants with

very different critical micelle concentrations (cmc). As a result, the growth of micelles, and an abrupt transition to bilayer disks and vesicles, was recently observed in a dilution path for mixtures of the single-chain surfactant dodecyltrimethylammonium bromide (DTAB, cmc = 15.4 mM) and the double-chain surfactant didodecyldimethylammonium bromide (DDAB, cmc = 0.085 mM).^{7,26} It was demonstrated that the mole fraction of surfactant in the aggregates may be accurately calculated using the Poisson–Boltzmann mean field theory for the electrostatic free energy of a charged interface.²⁶ Morphological changes, including a transition from micelles to vesicles, have also been frequently observed upon diluting mixtures of oppositely charged surfactants, for instance, mixtures of the anionic surfactant sodium dodecylsulfate (SDS) and the cationic surfactant DDAB,^{23,27} mixtures of SDS and DTAB,^{11–13} and

Received: May 17, 2013

Revised: July 31, 2013

Published: August 28, 2013

mixtures of sodium octylsulfate (SOS) and hexadecyltrimethylammonium bromide (CTAB).¹⁰

The structures of self-assembled aggregates in mixtures of SOS and CTAB have previously been investigated by Yatcilla et al.¹⁰ using cryo-transmission electron microscopy (cryo-TEM). Geometrically closed bilayer vesicles were observed in the dilute regimes in excess of either SOS or CTAB. The region where vesicles predominate was found to be considerably larger on the SOS-rich side. Moreover, small globular micelles were observed in more concentrated SOS-rich samples, and a transition to significantly larger vesicles was seen as the samples were diluted below about 1–2 wt %, depending on surfactant composition in solution. Notably, only small globular micelles could be observed in the cryo-TEM images for a few samples in the regime 0.75–1.7 wt %, despite the fact that the samples appeared bluish to the eye and dynamic light scattering (DLS) measurements indicated aggregates with a size in order of magnitude expected for vesicles and not micelles. It was also concluded that SOS-rich vesicles were considerably more flexible and nonspherically shaped as compared to CTAB-rich vesicles.

In this Article, we carry out a comprehensive investigation of the structural behaviors in SOS-rich mixtures of SOS and CTAB by means of comparing results from three experimental techniques, that is, small-angle neutron scattering (SANS), static light scattering (SLS), and cryo-TEM. Cryo-TEM is complementary to scattering methods in the sense that the latter occur *in situ*, and the information is measured in reciprocal space, whereas microscopy is measured *ex situ* and in direct space. In particular, we focus on the conspicuous discrepancy between results obtained from scattering techniques and cryo-TEM previously observed for the SOS/CTAB system. We have investigated two dilution paths on the SOS-rich side, which incorporate the growth from small spheroidal micelles to much larger bilayer structures.

This Article is organized as follows. Details about materials and experimental methods are given in the Experimental Section. In the section Model Calculations, we deal with detailed calculations based on the Poisson–Boltzmann theory of surfactant composition in bulk aggregates and concentrations of free surfactant monomers for SOS-rich mixtures of SOS and CTAB. The results obtained from these calculations enable us to rationalize many of our experimentally observed features. In the Results and Discussion, we present the results from our detailed model fitting analysis of SANS data. We also demonstrate, by comparing SANS (samples in D₂O) and SLS (samples in H₂O), that the choice of either H₂O or D₂O as solvent does not influence whether micelles or bilayers are present in a particular sample. Finally, we compare results obtained from the two types of experimental techniques, cryo-TEM, on the one hand, and scattering techniques (SANS and SLS), on the other hand, and demonstrate that there is a conspicuous discrepancy between the two sets of techniques with respect to whether micelles or bilayers are present in a particular sample.

EXPERIMENTAL SECTION

Materials. Sodium octyl sulfate (>95%, GC) and hexadecyltrimethylammonium bromide (>98%, GC) were obtained from Sigma and used without further purification. Deuterium oxide (D₂O) with 99.9 atom % D was purchased from Aldrich Chemical Co. Deionized ultrapure H₂O with resistivity 18.2 MΩ cm⁻¹ was received from a Milli-Q water purification unit.

Sample Preparation. Stock solutions containing sodium octyl sulfate (SOS) and hexadecyltrimethylammonium bromide (CTAB) with surfactant compositions equal to $y \equiv [SOS]/([SOS] + [CTAB]) = 0.90$ and 0.95 were prepared by simply mixing the surfactants with water to yield an overall surfactant concentration $c_t = [SOS] + [CTAB] = 160$ mM. The final samples were obtained by means of diluting the stock solutions to obtain a range of total surfactant concentration from $c_t = 10$ to 160 mM at ambient temperature (23 °C). Deuterium oxide (D₂O) was chosen as solvent in small-angle scattering measurements to minimize the incoherent background from hydrogen and obtain a high scattering contrast.²⁸ All samples were equilibrated at least 48 h before being measured at room temperature (23 °C). Notably, SOS-rich mixtures of SOS and CTAB are completely soluble in deuterium oxide at room temperature, although CTAB, as well as CTAB-rich mixtures, precipitates in D₂O below about 30 °C.

Methods. The small-angle neutron scattering (SANS) experiments were carried out at the D11 SANS instrument at Institut Laue-Langevin (ILL), Grenoble, France. A range of scattering vectors q from 0.002 to 0.44 Å⁻¹ was covered by three sample-to-detector distances (1.2, 8, and 39 m) at the neutron wavelength 4.6 Å. The setting with 8 m sample-to-detector distance was used as the reference setting for the absolute scale. The wavelength resolution was 10% (full width at half-maximum value).

The samples were kept in quartz cells (Hellma) with path lengths of 1 or 2 mm. The raw spectra were corrected for background from the solvent, sample cell, and other sources by conventional procedures.²⁹ The SANS data were set to absolute scale units and normalized by means of dividing with the concentrations in [g mL⁻¹] of aggregated surfactant (SOS and CTAB) as calculated according to a procedure described in Model Calculations, giving the unit [mL g⁻¹ cm⁻¹] for the normalized scattering cross section.

Because of the comparatively large amount of free monomers that are present in the solutions coexisting with self-assembled aggregates (see further below), we may express the latter quantity as a sum of two contributions:

$$\frac{d\sigma_m(q)}{d\Omega} \equiv \frac{1}{c_{agg}} \frac{d\sigma(q)}{d\Omega} = I_{agg}(q) + I_{mon}(q) \quad (1)$$

where

$$I_{agg}(q) = \Delta\rho_m^2 M_w P(q) [1 + \beta(q)(S(q) - 1)] \quad (2)$$

is the normalized absolute scattering intensity for a sample of weakly interacting dispersed aggregates and

$$I_{mon}(q) = \Delta\rho_{SOS}^2 M_{SOS} P_{surf}(q) \quad (3)$$

is the corresponding quantity for free surfactant monomers (SOS in SOS-rich mixtures, see further below). $\Delta\rho_m$ is the difference in scattering length per unit mass solute between particles with a homogeneous core and solvent, M_w is the molar mass of a bulk aggregate, and $P(q)$ is the form factor. $\Delta\rho_{SOS}$, M_{SOS} , and P_{surf} are the corresponding quantities for free surfactant monomers.

In the model fitting analysis, we have neglected interaggregate interactions and, consequently, set the structure factor $S(q)$ equal to unity unless the quality of the model fits otherwise could be significantly improved. Thus, it was found necessary to take into account interactions only for the most concentrated samples that consist of fairly monodisperse globular micelles. For these samples, a structure factor $S(q)$ as derived by Hayter and Penfold³⁰ from the Ornstein–Zernike equation in the rescaled mean spherical approximation³¹ was used in combination with the decoupling approximation^{32,33} in accordance with eq 2. The introduction of the Hayter–Penfold structure factor introduces three additional fitting parameters related to concentration of bulk aggregates, charge density in aggregates, and electrolyte concentration, respectively (see further below).

The average excess scattering length density per unit mass of solute (i.e., scattering length density divided by density of solute³⁴) for SOS

in D₂O, $\Delta\rho_{\text{SOS}} = -4.52 \times 10^{10} \text{ cm/g}$, was calculated using the appropriate molecular volume $\hat{v}_{\text{SOS}} = 302 \text{ \AA}^3$ and molecular weight $M_{\text{SOS}} = 232.3 \text{ g/mol}$. The molecular volume of SOS was calculated by means of subtracting the volume of an aliphatic butylene group^{35,36} ($-\text{CH}_2-\text{CH}_2-\text{CH}_2-\text{CH}_2-$) from the measured value for sodium dodecyl sulfate.³⁷ The corresponding quantities for CTAB are $\Delta\rho_{\text{CTAB}} = -6.66 \times 10^{10} \text{ cm/g}$, $\hat{v}_{\text{CTAB}} = 599 \text{ \AA}^3$, and $M_{\text{CTAB}} = 364.4 \text{ g/mol}$.³⁷ For the purpose of normalization of SANS data, we have set the scattering length density per unit mass of surfactant for mixed micelles equal to $\Delta\rho_m = x\Delta\rho_{\text{SOS}} + (1-x)\Delta\rho_{\text{CTAB}}$, where the mole fraction of SOS in the aggregates (x) is calculated according to a procedure described in Model Calculations.

Throughout the data analysis, corrections were made for instrumental smearing. For each instrumental setting, the ideal model scattering curves were smeared by the appropriate Gaussian resolution function when the model scattering intensity was compared to the measured absolute scale intensity in least-squares model fitting data analysis.^{38,39}

The parameters in the model were optimized by means of conventional least-squares analysis, and the quality of the fits was measured in terms of the reduced chi-squared parameter (χ^2).^{34,40} The quality of our model fits is exceptionally good with a reduced chi-squared always below $\chi^2 = 10$ and in the majority of fits below 5. In our model fitting analysis, we have always been careful to keep the number of fitting parameters at a minimum required to obtain good agreement between model and data, and never introduce additional fitting parameters unless the quality of the fit is significantly improved. The statistical errors of the parameters were calculated according to conventional methods.^{34,40} The different form factors and detailed models employed in the least-squares model fitting data analysis are given in the Supporting Information.

Static light scattering (SLS) measurements were carried out with a BI-200SM goniometer from Brookhaven Instruments attached to a water-cooled Lexel 95-2 laser with maximum power of 2 W and wavelength 514.5 nm. Experiments were carried out at 29 different angles in the range of $15^\circ \leq \theta \leq 155^\circ$, corresponding to q values in the range of $4.26 \times 10^{-4} \text{ \AA}^{-1} \leq q \leq 31.8 \times 10^{-4} \text{ \AA}^{-1}$. For each angle, the sample was measured a maximum of 15 individual times, out of which the five with the lowest intensities were picked out and subsequently averaged. The data were then normalized to absolute scale intensities using toluene as a reference standard.

The normalized light scattering intensity $K_c I(q)/c_{\text{agg}} K_{\text{SLS}}$ was plotted versus q , where c_{agg} is the concentration of surfactant in bulk aggregates. This gives the apparent molar mass $M_{\text{app}} \approx S(q=0)\langle M_w \rangle = \lim_{q \rightarrow 0} K_c I(q)/c_{\text{agg}} K_{\text{SLS}}$ when extrapolating the data to $q = 0$. $S(0) \approx 1$ at comparatively low values of c_{agg} in the presence of a substantial amount of electrolyte. The static light scattering constant is defined as

$$K_{\text{SLS}} = \frac{4\pi^2 n^2}{N_A \lambda^4} \left(\frac{dn}{dc} \right)^2 \quad (4)$$

where the refractive index of an aqueous solution is $n = 1.335$ at the appropriate laser light wavelength $\lambda = 514.5 \text{ nm}$. The refractive index increment was measured with a differential refractometer (Wyatt Optilab DSP) and was found to equal $dn/dc = 0.163 \text{ mL/g}$ for CTAB and $dn/dc = 0.119 \text{ mL/g}$ for SOS at the appropriate laser light wavelength. The average scattered intensity of a sample $I(q)$ is related to the scattering cross section (or Rayleigh ratio) by the scattering contrast constant, defined as

$$K_c = \frac{R_\theta}{I(q)} = \frac{R_\theta^{\text{ref}}}{I_{\text{ref}}} \left(\frac{n}{n_{\text{ref}}} \right)^2 \quad (5)$$

Toluene was used a reference for which $n_{\text{ref}} = 1.502$ and $R_\theta^{\text{ref}} = 32 \times 10^{-6} \text{ cm}^{-1}$ at $\lambda = 514.5 \text{ nm}$.^{41,42}

The aggregation numbers of micelles N_{SLS} were obtained by fitting normalized SLS data with a Guiner function, that is:

$$\frac{R_\theta}{c_{\text{agg}} K_{\text{SLS}}} = M_{\text{app}} e^{-(R_g q)^2/3} \quad (6)$$

and dividing by the appropriate average surfactant molecular volume:

$$N_{\text{SLS}} = \frac{M_{\text{app}}}{x\hat{v}_{\text{SOS}} + (1-x)\hat{v}_{\text{CTAB}}} \quad (7)$$

The resulting values of N_{SLS} are given in Table 2 in the Results and Discussion.

The cryo-TEM measurements were carried out at Uppsala University, Uppsala, Sweden using either a Zeiss EM 902A or a Zeiss Libra 120 transmission electron microscope (Carl Zeiss NTS, Oberkochen, Germany). Analysis was performed under cryo-conditions, and the microscope was operating at 80 kV and in zero loss bright-field mode. Digital images were recorded under low dose conditions with a BioVision Pro-SM Slow Scan CCD camera (Proscan GmbH, Scheuring, Germany) and iTEM software (Olympus Soft Imaging System, GmbH, Münster, Germany). Resolutions of the images were 15 and 19 Å/pixel, respectively, for the two instruments. To visualize as many details as possible, an underfocus of approximately 2 μm was used to enhance the image contrast.⁴³

Prior to imaging, the samples were treated by means of placing a drop of the aqueous solution on a grid with a holey polymer film (hole size ~2–6 μm) and then thinned by blotting it with some filter paper. This was done in an environmental chamber custom built for conditions close to 100% humidity to avoid dehydration of the sample. Once blotted, the sample was quickly vitrified in liquid ethane held at a temperature just above its freezing point (−183 °C). After vitrification, the sample was transferred to the microscope while keeping it cold with liquid nitrogen and avoiding air contact with the sample.

MODEL CALCULATIONS

Surfactant mixtures differ from pure surfactant systems in the way that an extra degree of freedom in terms of composition always appears. This may have a decisive influence on the structural behavior of self-assembled aggregates. Micelles or bilayers always coexist in equilibrium with free surfactant molecules, and, in a binary surfactant mixture, the aqueous free concentrations of the two surfactants may differ considerably from one another. As a result, the surfactant composition in the solution (y) must, in general, be different from the composition in the aggregates (x) at sufficiently dilute concentrations.²⁶

The free surfactant monomer concentrations and aggregate compositions may be calculated using the relations $c_1^{\text{free}} = \gamma_1 x \text{cmc}_1$ and $c_2^{\text{free}} = \gamma_2 (1-x) \text{cmc}_2$, where cmc_1 and cmc_2 are the critical micelle concentrations (cmc) of surfactant 1 (SOS) and surfactant 2 (CTAB), respectively.²⁶ The mole fraction of surfactant 1 in the aggregates (x) may be calculated for a given total surfactant concentration $c_t = c_{\text{agg}} + c_1^{\text{free}} + c_2^{\text{free}}$ and mole fraction of surfactant 1 in solution, $y = (c_1^{\text{free}} + x c_{\text{agg}})/c_t$, from given values of the two activity coefficients γ_1 and γ_2 . The above equations are generally valid for any binary surfactant mixture, and detailed expressions of γ_1 and γ_2 may be derived from an appropriate detailed model for a specified type of surfactant mixture. It was recently demonstrated that γ_1 and γ_2 , as derived for mixtures of two cationic surfactants using the Poisson–Boltzmann (PB) mean field theory for the free energy of the electrostatic double layer, may generate accurate values for x , c_{agg} , c_1^{free} , and c_2^{free} .²⁶ In this work, we have employed the appropriate relations for a mixture of an anionic and a cationic surfactant as previously derived by Bergström.⁴⁴ More details, including detailed expressions of γ_1 and γ_2 for mixtures of an anionic and a cationic surfactant, are given in the Supporting Information.

It follows from the above relations together with PB calculations that, in a mixture of two oppositely charged surfactants with cmc in the same order of magnitude, the concentration of free surfactant will be much higher for the

surfactant in excess than for the surfactant in deficit. This is in agreement with experimental observations.^{11,12,45} The difference in free monomer concentrations between the two surfactants is even more emphasized in our particular system of SOS-rich mixtures of SOS and CTAB, because the critical micelle concentration of pure SOS ($\text{cmc}_1 = 133 \text{ mM}$)^{46,47} is much higher than that for CTAB ($\text{cmc}_2 = 0.9 \text{ mM}$).^{48,49} Outcomes of our calculations for the various samples investigated in this Article are tabulated in the Supporting Information.

The concentrations of free surfactant monomers as well as surfactant aggregated in micelles or bilayers, as calculated from the procedure described above, are plotted in Figure 1 as a

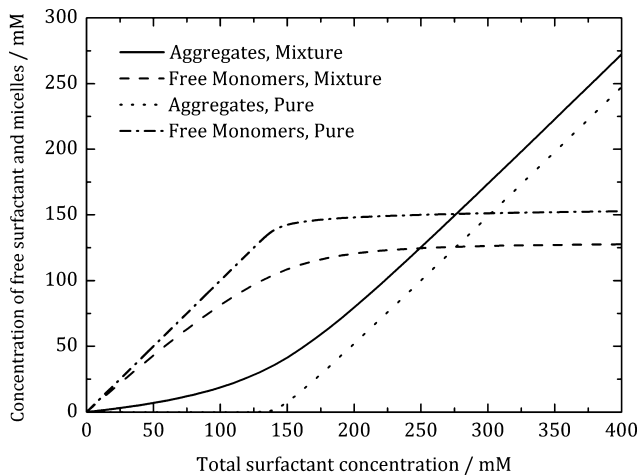


Figure 1. The concentration of surfactants in aggregates (—) and free surfactants (---) for a mixture of SOS and CTAB, as calculated from the Poisson–Boltzmann theory, plotted against the total surfactant concentration $c_t \equiv [\text{SOS}] + [\text{CTAB}]$ at a fixed surfactant composition $y \equiv [\text{SOS}] / ([\text{SOS}] + [\text{CTAB}]) = 0.95$ in solution. For the sake of comparison, we have also plotted the corresponding quantities for pure SOS ($\text{cmc}_1 \approx 133 \text{ mM}$), that is, the concentration of surfactants in aggregates (---) and free surfactants (----).

function of total surfactant concentration for a given mole fraction of SOS in the solution $y = [\text{SOS}] / ([\text{SOS}] + [\text{CTAB}]) = 0.95$. For the sake of comparison, we have also plotted the corresponding functions for pure SOS with cmc set to $\text{cmc}_1 = 133 \text{ mM}$.^{50,51} It is seen that surfactant mixtures behave fundamentally different from pure surfactant systems in the way that an appreciable amount of aggregates coexists with free monomers in a wide range of dilute surfactant concentrations, that is, below about cmc for pure surfactant 1 (SOS). In the present work, we have investigated samples as concentrated as $[\text{SOS}] + [\text{CTAB}] = 160 \text{ mM}$. Nevertheless, it turns out that the concentration of free monomers is always higher than the concentration of surfactant aggregated in micelles and bilayers [cf., Figure 1].

In general, the regime where free monomers predominate over bulk aggregates is found to be about twice the cmc for the pure surfactant in excess (that is, cmc_1 in our present case of SOS-rich samples), and the regime where the surfactant mole fraction in aggregates (x) is significantly different from the mole fraction in solution (y) extends to about 10 times cmc_1 . This means that the situation must be rather different in CTAB-rich solutions for which $\text{cmc}_2 \approx 1 \text{ mM}$, and the amount of free surfactant only predominates below about 2 mM.

The concentrations of aggregates and free monomers for a pure surfactant system (dotted and dash-dotted lines for the case of SOS shown in Figure 1) were calculated according to a procedure described in detail elsewhere⁵¹ as well as in the Supporting Information. Notably, the free monomer concentration increases with increasing total surfactant concentration above cmc for both pure and mixed systems. The reason for this is that the chemical potential of surfactant in micelles increases as the entropy of mixing micelles and solvent decreases with increasing solute concentration. As a result, the chemical potential of free surfactant must also increase in accordance with the condition of equilibrium between free and aggregated surfactants, and so must the concentration of free monomers.^{50,51}

The fraction of surfactant that is present in aggregates decreases as the total surfactant concentration is decreased. As a consequence of the fact that virtually only SOS is present as free monomers in SOS-rich samples, the composition in the aggregates changes dramatically with total surfactant concentration. In Figure 2, the mole fraction of SOS in the aggregates

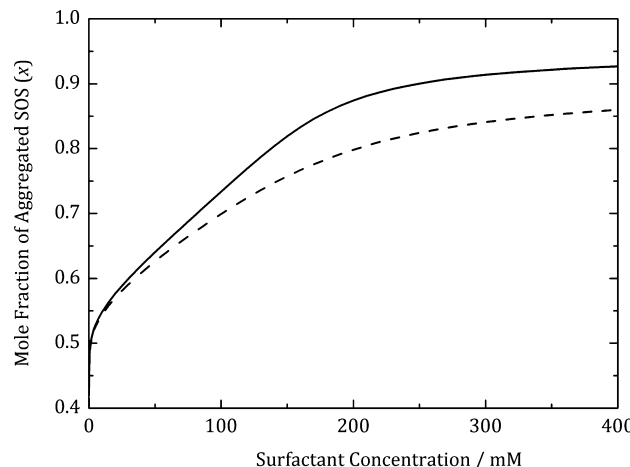


Figure 2. The mole fraction of aggregated anionic surfactant SOS, as calculated from the Poisson–Boltzmann theory, plotted against the overall surfactant concentration in solution $c_t \equiv [\text{SOS}] + [\text{CTAB}]$ for an overall SOS mole fraction in solution $y \equiv [\text{SOS}] / ([\text{SOS}] + [\text{CTAB}]) = 0.95$ (—) and $y = 0.90$ (----).

(x) is plotted against the total surfactant concentration at a fixed surfactant mole fraction in solution ($y = 0.95$). It is seen that, upon simply diluting a sample at a given total surfactant concentration, x decreases from a value close to the mole fraction in solution and approaches a value close to equimolar composition. As a result of the considerable change in x , we are able to observe evident structural changes of the self-assembled surfactant bulk aggregates, and below we report the sequence of microstructural transformations from small spheroidal or ellipsoidal micelles to large bilayer structures (vesicles and disks) as our samples are progressively diluted at given values $y = 0.90$ and 0.95 .

RESULTS AND DISCUSSION

SANS Measurements of SOS-Rich Samples. We have measured samples with different surfactant concentrations at two mole fractions, $y \equiv [\text{SOS}] / ([\text{SOS}] + [\text{CTAB}]) = 0.90$ and 0.95 , and the results from the least-squares model fitting analysis are given in Table 1. Examples of SANS data with

Table 1. Results from Least-Square Model Fitting Analysis of SANS Data^a

	160 mM	140 mM	120 mM	100 mM	80 mM	60 mM	40 mM	20 mM	10 mM
$y = 0.90$	micelles		micelles	micelles	bilayers		bilayers	bilayers	bilayers
$a = 17.5$		$a = 16.4$	$a = 17.0$	$f_d = 0.41$		$f_d = 0.33$	$f_d = 0.28$	$f_d = 0.28$	
$b = 23.4$		$b = 23.7$	$b = 22.9$	$f_v = 0.59$		$f_v = 0.67$	$f_v = 0.72$	$f_v = 0.72$	
$c = 29.5$		$\langle L \rangle = 64.0$	$\langle L \rangle = 504$	$\xi = 14.3$		$\xi = 15.2$	$\xi = 15.8$	$\xi = 15.6$	
$l_s = 15$		$l_s = 20$	$l_s = 19$	$R_d \approx 1000$		$R_d > 1000$	$R_d > 1000$	$R_d > 1000$	
$\alpha = 0.17$		$\sigma_L/\langle L \rangle = 0.80$	$\sigma_L/\langle L \rangle = 0.60$	$R_v = 310$		$R_v = 330$	$R_v = 350$	$R_v = 290$	
$c_{el} = 50 \text{ mM}$				$\sigma_v/R_v = 0.60$		$\sigma_v/R_v = 0.55$	$\sigma_v/R_v = 0.55$	$\sigma_v/R_v = 0.70$	
$c_{mic} = 90 \text{ mM}$				$l_s = 18$		$l_s = 19$	$l_s = 19$	$l_s = 18$	
$y = 0.95$	micelles	micelles	micelles	micelles	micelles and bilayers	bilayers	bilayers	bilayers	
$a = 14.7$	$a = 16.5$	$a = 17.9$	$a = 16.6$	$f_m = 0.12$	$f_d = 0.51$	$f_d = 0.44$			$f_d = 0.46$
$b = c = 23.0$	$b = 22.4$	$b = 23.3$	$b = 23.8$	$f_d = 0.14$	$f_v = 0.49$	$f_v = 0.56$			$f_v = 0.54$
$l_s = 14$	$c = 26.8$	$c = 30.9$	$\langle L \rangle = 55.1$	$f_v = 0.74$	$\xi = 14.5$	$\xi = 15.3$			$\xi = 16.1$
$\alpha = 0.26$	$l_s = 14$	$l_s = 14$	$l_s = 16$	$r_c = 20.3$	$R_d \approx 1000$	$R_d \approx 1000$			$R_d \approx 900$
$c_{el} = 100 \text{ mM}$	$\alpha = 0.15$	$\alpha = 0.06$	$\sigma_L/\langle L \rangle = 0.85$	$\xi = 13.8$	$R_v = 300$	$R_v = 280$			$R_v = 280$
$c_{mic} = 70 \text{ mM}$	$c_{el} = 70 \text{ mM}$	$c_{el} = 30 \text{ mM}$		$R_d = 500$	$\sigma_v/R_v = 0.55$	$\sigma_v/R_v = 0.55$			$\sigma_v/R_v = 0.50$
	$c_{mic} = 70 \text{ mM}$	$c_{mic} = 80 \text{ mM}$		$R_v = 420$	$l_s = 16$	$l_s = 17$			
				$\sigma_v/R_v = 0.45$					
				$l_s = 16$					

^aDimensional properties (a , b , c , ξ , $\langle L \rangle$, R_v , R_d , and l_s) are given in units of angstrom (Å). Denotations for the different quantities are defined in Appendix A. The fitting parameters α , c_{el} , and c_{mic} in the case of ellipsoidal micelles, are all related to the structure factor, taking into account repulsive intermicellar interactions.

model fits for the dilution series at $y = 0.95$ are given in Figure 3 and at $y = 0.90$ in Figure 4. The conspicuous difference in appearance of SANS data for samples containing micelles or bilayer aggregates, respectively, is clearly seen in Figures 3 and 4. The presence of large bilayer structures in the most diluted samples is evident from the strong increase in normalized scattering intensity with decreasing q according to a slope proportional to q^{-2} in a logarithmic plot.

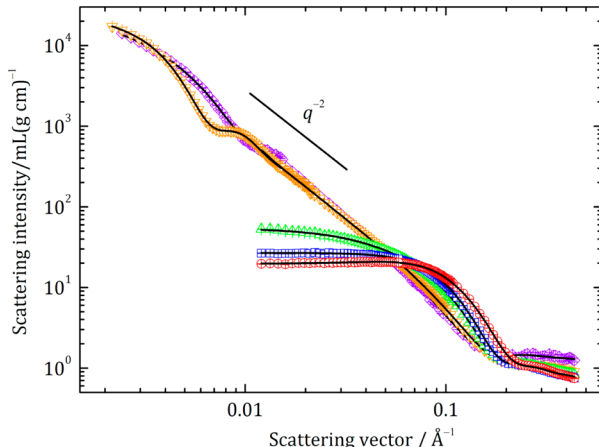


Figure 3. Normalized scattering cross section as a function of the scattering vector q for mixtures of SOS and CTAB in deuterium oxide for a given mole fraction of SOS in solution $y \equiv [\text{SOS}]/([\text{SOS}] + [\text{CTAB}]) = 0.95$. The overall surfactant concentrations of the samples are $c_t \equiv [\text{SOS}] + [\text{CTAB}] = 160 \text{ mM} (\circ)$, $c_t = 120 \text{ mM} (\square)$, $c_t = 100 \text{ mM} (\triangle)$, $c_t = 80 \text{ mM} (\nabla)$, and $c_t = 10 \text{ mM} (\diamond)$. Symbols represent SANS data obtained for different sample-detector distances. The solid lines represent the best available fit with a model for oblate spheroids (\circ), general ellipsoids (\square), polydisperse rods with an elliptical cross section (\triangle), coexisting bilayer disks, bilayer vesicles, and rodlike micelles (∇), and coexisting disks and vesicles (\diamond). The results of the fits are given in Table 1. The mole fraction of aggregated SOS, as calculated from the Poisson-Boltzmann theory, is $x = 0.84$ (\circ), $x = 0.78$ (\square), $x = 0.73$ (\triangle), $x = 0.70$ (∇), and $x = 0.55$ (\diamond).

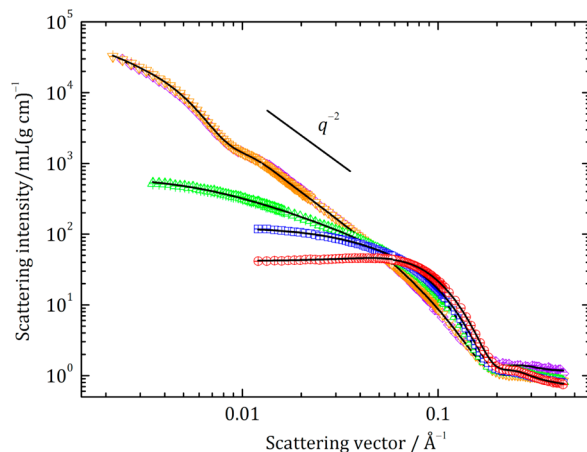


Figure 4. Normalized scattering cross section as a function of the scattering vector q for mixtures of SOS and CTAB in deuterium oxide for a given mole fraction of SOS in solution $y \equiv [\text{SOS}]/([\text{SOS}] + [\text{CTAB}]) = 0.90$. The overall surfactant concentrations of the samples are $c_t \equiv [\text{SOS}] + [\text{CTAB}] = 160 \text{ mM} (\circ)$, $c_t = 120 \text{ mM} (\square)$, $c_t = 100 \text{ mM} (\triangle)$, $c_t = 80 \text{ mM} (\nabla)$, and $c_t = 10 \text{ mM} (\diamond)$. Symbols represent SANS data obtained for different sample-detector distances. The solid lines represent the best available fits with a model for general ellipsoids (\circ), polydisperse rods with an elliptical cross section (\square and \triangle), and coexisting bilayer disks and vesicles (∇ and \diamond). The results of the fits are given in Table 1. The mole fraction of aggregated SOS, as calculated from the Poisson-Boltzmann theory, is $x = 0.77$ (\circ), $x = 0.73$ (\square), $x = 0.71$ (\triangle), $x = 0.67$ (∇), and $x = 0.54$ (\diamond).

The SANS data were normalized by means of dividing the absolute intensity by the concentration of surfactants that form aggregates, as calculated from the Poisson-Boltzmann theory and tabulated in the Supporting Information. The accuracy of the calculations is supported by the fact that the SANS data for different surfactant concentrations fall on top of one another in the high- q regime, when this procedure is employed to normalize the data. On the other hand, if the data are normalized in accordance with the more conventional

procedure of dividing with respect to the total surfactant concentration (aggregates + free monomers), there is an evident progression of decreasing normalized scattering intensity with decreasing total surfactant concentration [cf, Figure S2 in the Supporting Information].

Micelles. The micelles in the sample [$y = 0.95$, 160 mM] are found to be shaped as rather small oblate spheroids with half axes $a = 14.7 \text{ \AA}$ and $b = 22.9 \text{ \AA}$, and they grow mainly in the length direction to form general ellipsoids with half axes $a < b < c$ upon diluting the sample to 140 and 120 mM, respectively. A similar growth of micelles from small oblate spheroids to elongated ellipsoids has previously been observed in mixtures of the two oppositely charged surfactants sodium dodecyl sulfate (SDS) and dodecytrimethylammonium bromide (DTAB),^{11,52} as well as in mixtures of a single-chain (DTAB) and a double-chain (DDAB) cationic surfactant.^{7,53} In addition, we find ellipsoidal micelles in the sample [$y = 0.90$, 160 mM]. The statistical errors of the half axes a and b , as obtained from the SANS data analysis, are always less than $\pm 0.5 \text{ \AA}$ and of c always less than $\pm 1 \text{ \AA}$.

The SANS data for the four samples with spheroidal or ellipsoidal micelles could not at all be fitted unless a structure factor $S(q)$, incorporating repulsive excluded volume interactions as well as electrostatic double-layer forces,^{30,33} was employed. This structure factor introduces three additional fitting parameters: (i) the relative effective charge of the micelles ($\alpha = z_{\text{eff}}/z_{\text{id}}$), (ii) the electrolyte concentration (c_{el}), and (iii) the concentration of surfactant aggregated in micelles (c_{mic}). More details are given in the Supporting Information. The values obtained from the model fitting analysis are given in Table 1 and may be compared to the corresponding values (c_{agg} and c_{free}) as calculated from the Poisson–Boltzmann theory and tabulated in the Supporting Information. In accordance, we obtain c_{el} and c_{mic} of reasonable order of magnitudes, although the structure factor is derived for the case of strictly spherical geometry with charge densities considerably lower than expected for the micelles in these samples. The discrepancy between c_{free} and c_{el} and between c_{agg} and c_{mic} , respectively, is less than a factor of 2 except for one of the samples for which the difference is about a factor of 3.

In more dilute samples, the influence of structure factor effects on the SANS data appears to be weaker, and the scattering data could be satisfactorily fitted by means of setting $S(q) = 1$. The comparatively weak interactions found in SOS-rich mixtures of SOS and CTAB are mainly due to the presence of relatively large amounts of free ionic surfactant shielding the electrostatic double layer interactions. Moreover, interaggregate interactions are expected to rapidly become weaker as the samples are diluted, not only because the bulk aggregate volume fraction decreases, but also because the surface charge density decreases as a result of the surfactant mole fraction (x) approaching equimolar composition. Notably, the surface charge of bulk aggregates is canceled out as two oppositely charged surfactants are aggregated, and $x = 0.5$ corresponds to completely uncharged bulk aggregates.

It was also found that the bare models of ellipsoidal or spheroidal micelles could not fit the data at high- q values, that is, $q \gtrsim 0.2 \text{ \AA}^{-1}$ [cf, Figure 5]. Introducing a core–shell structure in the model could not improve the agreement between model and data. However, excellent agreement between data and model was obtained as the presence of large amounts of free surfactant molecules were taken into account. An example of SANS data with fits using models

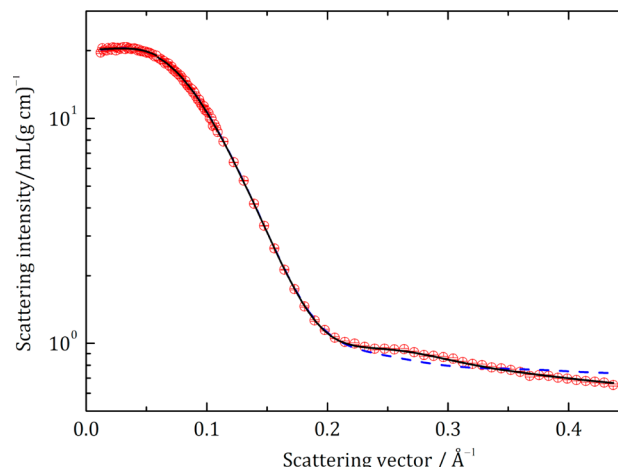


Figure 5. Normalized scattering cross section as a function of the scattering vector q for mixtures of SOS and CTAB in deuterium oxide in the absence of added salt for a given mole fraction of SOS in solution $y \equiv [\text{SOS}] / ([\text{SOS}] + [\text{CTAB}]) = 0.95$ and an overall surfactant concentration of the samples $[\text{SOS}] + [\text{CTAB}] = 140 \text{ mM}$. Symbols represent SANS data obtained for different sample–detector distances. The solid line represents the best available fit with a model for general ellipsoids coexisting with free monomer models as infinitely thin short rigid rods. The dashed line represents the best available fit with a model for general ellipsoids ignoring the presence of free surfactant. The quality of the fits as measured by χ^2 is 2.6 (—) and 14.8 (---).

including as well as excluding free monomers is shown in Figure 5 for the sample [$y = 0.95$, 140 mM].

The free surfactants were modeled with a form factor for infinitely thin rods with length l_s in accordance with eq 3. It was not possible to determine both l_s and the mass fraction of free surfactant from the model fitting analysis because the two parameters appeared to be strongly intercorrelated. For this reason, we have fixed the latter parameter to the value obtained from our theoretical calculations based on the Poisson–Boltzmann theory. For instance, the sample shown in Figure 5 consists of 37 mM surfactant aggregated in micelles and 103 mM free surfactant (SOS) according to our calculations; that is, only about 25% of the surfactants are incorporated in micelles. The fraction of free monomers is found to increase with decreasing total surfactant concentration in accordance with our model calculations, and the presence of free monomers was necessary to take into account for all of our data.

The obtained values of l_s are found to be in the range 14–19 Å, which should be compared to the length 15.4 Å of a fully stretched octyl chain. Notably, virtually all free surfactant consists of the surfactant in excess (that is SOS in SOS-rich mixtures), and the headgroup of SOS is invisible with SANS in a solvent of deuterium oxide.⁵⁴ The statistical errors for l_s are about $\pm 3 \text{ \AA}$ for micellar samples and $\pm 5 \text{ \AA}$ for samples containing bilayers. This implies relative errors of l_s that are considerably larger in magnitude as compared to the residual fitting parameters (see further below).

The presence of free surfactant is even more evident in the more diluted samples that contain bilayer structures, because the fraction of surfactant present as free surfactants increases in magnitude as the total surfactant concentration is decreased [cf, Figure 1]. As a matter of fact, an increasing mass fraction of free surfactant with decreasing surfactant concentration is evident from the scattering data shown in Figures 3 and 4 as an

increase in normalized scattering intensity in the high- q regime with decreasing surfactant concentration. This means that we, indeed, are able to observe and confirm, from the behavior of SANS data, the presence of comparatively large amounts of free surfactant molecules in the investigated samples.

As the samples are further diluted, the micelles grow considerably in length, and the corresponding data, that is, for the samples [$y = 0.90$, 120 mM], [$y = 0.90$, 100 mM], and [$y = 0.95$, 100 mM], were best fitted with a model for polydisperse rigid rods with a volume-averaged length $\langle L \rangle$ and an elliptical cross section with half axes a and b . The longest rodlike micelles were found in the sample [$y = 0.90$, 100 mM] with an average length $\langle L \rangle \approx 500 \pm 15 \text{ \AA}$. The polydispersity of the micelles expressed in terms of the relative standard deviation $\sigma_L/\langle L \rangle$ is found to be in the range 0.6–0.85, with a statistical error about ± 0.05 . Intermicellar interactions were neglected in our analysis of polydisperse rods, and, as a consequence, the average micelle length $\langle L \rangle$ as obtained from our data analysis is expected to be somewhat smaller than the real length of the micelles, whereas $\sigma_L/\langle L \rangle$ is expected to be somewhat underestimated.^{11,55}

In Table 2 we have given the aggregation number of micelles (N or $\langle N \rangle$) in D₂O as calculated from the dimensional

Table 2. Aggregation Numbers Determined with Two Different Approaches with SANS (N and N' , D₂O as Solvent) and SLS (N_{SLS} , H₂O as Solvent)

	160 mM	140 mM	120 mM	100 mM
$y = 0.90$	$N = 140$	Not measured	$\langle N \rangle = 200$	$\langle N \rangle = 1590$
	$N' = 140$	Not measured	$N' = 270$	$N' = 1480$
	$N_{SLS} = 79$	$N_{SLS} = 110$	$N_{SLS} = 240$	$N_{SLS} = 1510$
$y = 0.95$	$N = 92$	$N = 120$	$N = 150$	$\langle N \rangle = 180$
	$N' = 90$	$N' = 94$	$N' = 130$	$N' = 220$
	$N_{SLS} = 100$	$N_{SLS} = 94$	Not measured	$N_{SLS} = 320$

properties obtained from the model fitting analysis (a , b , c , or $\langle L \rangle$), the appropriate surfactant molecular weights, $\hat{\nu}_{\text{SOS}} = 302 \text{ \AA}^3$ and $\hat{\nu}_{\text{CTAB}} = 599 \text{ \AA}^3$, and the surfactant mole fraction as calculated from the PB theory and tabulated in the Supporting Information. Alternatively, the aggregation number (denoted N') can be calculated from the normalized absolute scale form factor scattering intensity in the limit $q \rightarrow 0$ by means of dividing by the appropriate surfactant molecular weights. In the latter procedure, we have taken into account the fact that a certain amount of surfactant, as discussed above, is not incorporated in the micelles. The two independent procedures give values of N and N' that are close to one another, which supports the validity and accuracy of our calculations of free surfactant concentrations. Because intermicellar interactions were neglected in the analysis of samples with polydisperse rodlike micelles, the tabulated aggregation numbers are expected to be somewhat smaller than the corresponding real quantities.

In Table 2 we have also included the aggregation numbers as obtained with static light scattering (denoted N_{SLS}) for samples prepared in H₂O. It is noted that the difference between estimated aggregation numbers in the two solvents H₂O and D₂O, respectively, is comparatively small, and no systematic trends with respect to the choice of solvent can be observed.

Bilayers. A transition from micelles to bilayers is observed as the total surfactant concentration reaches about $c_t = 80 \text{ mM}$

at both compositions $y = 0.90$ and 0.95. This transition from comparatively small micelles to much larger bilayers aggregates is abrupt in the sense that it is not continuous and that intermediate structures, or aggregates of intermediate size, are never observed. In addition, the regime where micelles and bilayers coexist is found to be narrow, similar to what we have previously found for other catanionic surfactant mixtures,^{12,27} and in contrast to mixtures of a single-tailed and a double-tailed cationic surfactant.⁷

The presence of vesicles in the bilayer containing samples is indicated by the presence of an elevation or weak oscillation in the SANS data at about $q = 0.01 \text{ \AA}^{-1}$ [cf., Figures 3, 4, and 6],

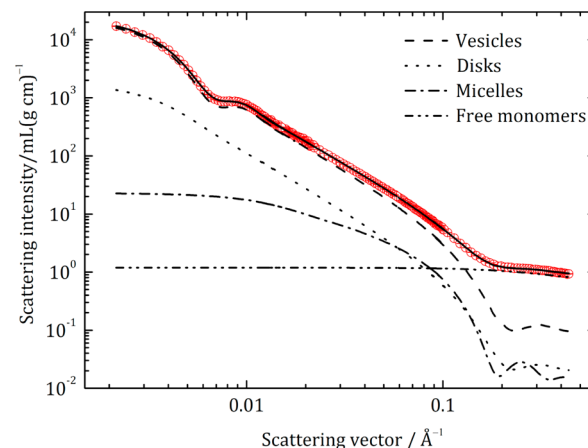


Figure 6. Normalized scattering cross section as a function of the scattering vector q for mixtures of SOS and CTAB in deuterium oxide in the absence of added salt for a given mole fraction of SOS in solution $y \equiv [\text{SOS}] / ([\text{SOS}] + [\text{CTAB}]) = 0.95$ and an overall surfactant concentration of the samples $[\text{SOS}] + [\text{CTAB}] = 80 \text{ mM}$ (○). Symbols represent SANS data obtained for different sample-detector distances. The solid line represents the best available fit with a model for coexisting bilayer vesicles (74%), disks (14%), and micelles (12%). Individual contributions from vesicles (— · — · —), disks (— · — · —), micelles (— · — · —), and free monomers (— · — · — · —) are also shown. Results from the least-squares model fitting analysis are given in Table 1. The quality of the fit as measured by the reduced chi-squared parameter χ^2 is 6.3.

and the exact location of it is related to the size of the vesicles. However, the SANS data for these samples could never be fitted with a model assuming only vesicles to be present in the samples, but only with a model for coexisting bilayer vesicles and disks.

Coexisting bilayers and micelles could only be observed in one of our samples, that is, [$y = 0.95$, 80 mM], with a fraction of micelles equal to $f_m = 0.12 \pm 0.02$ [cf., Figure 6]. In Figure 6 we have also included the individual contributions from the three aggregate types present, that is, vesicles, disks, and rodlike micelles, respectively, as well as the contribution from free monomers to the total scattering. The presence of micelles is seen as a slight increase in scattering intensity at about $q = 0.1 \text{ \AA}^{-1}$, whereas the presence of disks influences the scattering behavior mainly in the low- q regime, that is, below about $q = 0.01 \text{ \AA}^{-1}$.

Vesicles are found, in general, to predominate over disks; that is, the mass fraction of vesicles was found to be in the range $0.5 < f_v < 0.75$. The statistical error of f_v is always smaller than ± 0.05 . No clear trend of f_v with respect to surfactant concentration could be observed, except that the amount of

vesicles relative to disks is found to be much larger in the sample [$y = 0.95, 80 \text{ mM}$] shown in Figure 6, where bilayers are observed to coexist with micelles. The mass fraction of vesicles in the latter sample is 5 times higher than for disks, whereas the vesicle-to-disk ratio falls in the range 1–3 in the remaining samples. The considerable amount of vesicles present in the sample at [$y = 0.95, 80 \text{ mM}$] is evident from the comparatively sharp oscillation at $q \approx 0.01 \text{ \AA}^{-1}$ in the corresponding SANS data as compared to, for instance, SANS data for the sample [$y = 0.95, 10 \text{ mM}$] shown in Figure 3.

Notably, coexisting vesicles and disks was recently observed with SANS in mixtures of the two cationic surfactants dodecyltrimethylammonium bromide (DTAB) and didodecyl-dimethylammonium bromide (DDAB), but in this system bilayer disks were always seen to predominate over vesicles, that is, $0.6 < f_d < 1.0$, where $f_d = 1 - f_v$ is the mass fraction of disks.⁷

The vesicles are found to have a radius about $R_v \approx 300 \text{ \AA}$, with a statistical error about $\pm 5 \text{ \AA}$, and to be comparatively polydisperse with a relative standard deviation $\sigma_v/R_v \approx 0.6 \pm 0.03$. The disks appear to be larger, that is, $R_d \gtrsim 1000 \text{ \AA}$, but their exact size or polydispersity could not be determined from our SANS data due to lack of data below about $q = 0.002 \text{ \AA}^{-1}$. For one of the most diluted bilayer containing samples, that is, [$y = 0.90, 10 \text{ mM}$], the agreement between model and data could be significantly improved by assuming the vesicles to be perforated with holes. This issue will be further treated in a forthcoming paper.

The half bilayer thickness ξ is found to be in the range 13.8–16.1 \AA , with a statistical error of ξ always less than $\pm 0.3 \text{ \AA}$, and there is a clear trend of increasing ξ with decreasing surfactant concentration. This trend agrees very well with our expectation that the mole fraction of the surfactant with shortest tail (SOS) in the aggregates decreases with decreasing total surfactant concentration, as discussed above. As a consequence, we are able to estimate the surfactant composition in the bilayer aggregates by means of determining the constants ξ_1 (SOS) and ξ_2 (CTAB) from the linear relation $\xi = x\xi_1 + (1 - x)\xi_2$ for the two most concentrated samples containing bilayers, that is, [$y = 0.95, 80 \text{ mM}$] and [$y = 0.90, 80 \text{ mM}$], giving $\xi_1 = 9.9 \text{ \AA}$ and $\xi_2 = 23.2 \text{ \AA}$, and using these values to calculate x for the more diluted samples. The corresponding results (denoted x_{bil}) are summarized in Table 3 and compared to the values for the

Table 3. Mole Fraction of Aggregated SOS As Estimated from the Bilayer Thickness (x_{bil}) and Calculated from the PB Theory (x_{calc})

sample	x_{bil}	x_{calc}	sample	x_{bil}	x_{calc}
$y = 0.95, 60 \text{ mM}$	0.65	0.66	$y = 0.90, 40 \text{ mM}$	0.60	0.61
$y = 0.95, 40 \text{ mM}$	0.59	0.62	$y = 0.90, 20 \text{ mM}$	0.56	0.57
$y = 0.95, 10 \text{ mM}$	0.53	0.55	$y = 0.90, 10 \text{ mM}$	0.55	0.54

same quantity as calculated from the PB theory (denoted x_{calc}). It is seen that the two estimated values for the surfactant composition in the bilayer aggregates excellently agree with one another.

The abrupt transition from micelles to bilayers observed in the present work for SOS-rich mixtures of SOS and CTAB is similar to what has been observed in several related surfactant systems.^{5–7,12,27} Considering our observation that the transition occurs at [$y = 0.95, 80 \text{ mM}$], where micelles and bilayers are found to coexist, we are able to conclude, in accordance with

the model calculations of aggregate composition, that the micelle-to-bilayer transition in SOS-rich mixtures of SOS and CTAB occurs at a mole fraction of SOS in the aggregates equal to about $x = 0.70$. An abrupt transition from micelles to bilayers is, indeed, predicted from a theoretical model based on thermodynamics of self-assembly combined with bending elasticity properties of the self-assembled aggregates.^{56,57} In accordance, the micelle-to-bilayer transition is predicted to occur as the spontaneous curvature equals $H_0 = 1/4\xi$, where ξ is the thickness of the self-assembled monolayer interface (equivalent to half bilayer thickness). The spontaneous curvature is expected to be a strong function of surfactant composition, and it has previously been demonstrated that the micelle-to-bilayer transition is induced by changes in aggregate composition x .²⁶

Comparison between SANS and Cryo-TEM. In addition to the SANS measurements, we have also investigated samples prepared with water (H_2O) as solvent with cryo-TEM as well as static light scattering (SLS). With the latter technique, we are able to qualitatively distinguish between small micelles, large micelles, and bilayer aggregates [cf., Figure 7].

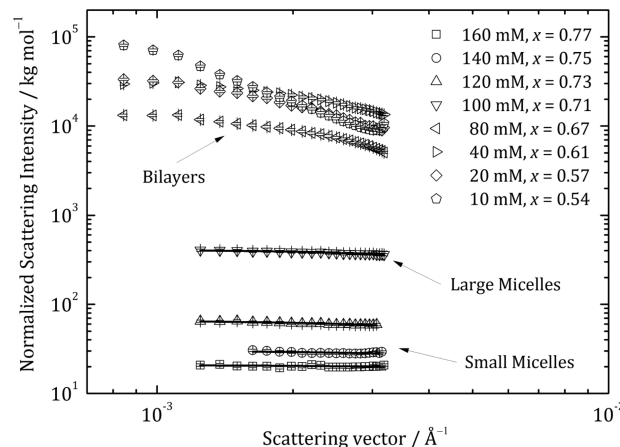


Figure 7. Normalized scattering intensity ($R_\theta/c_{\text{agg}}K_{\text{SLS}}$) as a function of the scattering vector q for samples with different overall surfactant concentrations for a given value of the mole fraction $y = 0.90$ of SOS in solution. Symbols represent data obtained with static light scattering (SLS). The mole fraction of aggregated SOS (x) as calculated from the PB theory is given for the different samples. The solid lines represent the best available fits with a Guiner function for samples containing micelles. The resulting aggregation numbers (N_{SLS}) are shown in Table 2.

In Tables 4 and 5, the qualitative outcome of the results from the three techniques cryo-TEM, SLS, and SANS is summarized and compared. It is evident that SANS (D_2O as solvent) and SLS (H_2O as solvent) always give identical results as to whether small micelles, large micelles, or bilayers are present in a particular sample. Moreover, the choice of H_2O or D_2O as solvent has no influence at all on the macroscopic appearance of the samples to the bare eye; that is, micellar samples always appear clear and bilayer samples bluish. Furthermore, considering the unusually rich structural behavior along the dilution paths (small globular micelles, large rodlike micelles, and much larger bilayer aggregates), we may conclude there is no significant difference in micelle aggregation numbers as obtained with SANS (D_2O as solvent) and SLS (H_2O as solvent), respectively [cf., Table 2]. As a consequence, we are

Table 4. Comparison of Results for the Three Experimental Techniques Cryo-TEM, SLS, and SANS for Samples with Composition Solution $y \equiv [SOS]/([SOS] + [CTAB]) = 0.95$

sample	cryo-TEM in H ₂ O and D ₂ O	SLS in H ₂ O	SANS in D ₂ O	appearance
$y = 0.95, 100\text{--}160\text{ mM}$	Not measured	small micelles	spheroidal, ellipsoidal, or short rodlike micelles	clear
$y = 0.95, 80\text{ mM}$	Not measured	bilayers	vesicles, disks, and micelles	bluish
$y = 0.95, 60\text{ mM}$	globular micelles	bilayers	vesicles and disks	bluish
$y = 0.95, 40\text{ mM}$	micelles, closed and open vesicles, disks	bilayers	vesicles and disks	bluish

Table 5. Comparison of Results for the Three Experimental Techniques Cryo-TEM, SLS, and SANS for Samples with Composition Solution $y \equiv [SOS]/([SOS] + [CTAB]) = 0.90$

sample	cryo-TEM in H ₂ O	SLS in H ₂ O	SANS in D ₂ O	appearance
$y = 0.90, 120\text{--}160\text{ mM}$	Not measured	small micelles	ellipsoidal or short rodlike micelles	clear
$y = 0.90, 100\text{ mM}$	Not measured	large micelles	long rodlike micelles	clear
$y = 0.90, 80\text{ mM}$	wormlike micelles	bilayers	vesicles and disks	bluish
$y = 0.90, 60\text{ mM}$	closed and open vesicles	bilayers	Not measured	bluish
$y = 0.90, 40\text{ mM}$	closed and open vesicles	bilayers	vesicles and disks	bluish
$y = 0.90, 20\text{ mM}$	closed and open vesicles	bilayers	vesicles and disks	bluish

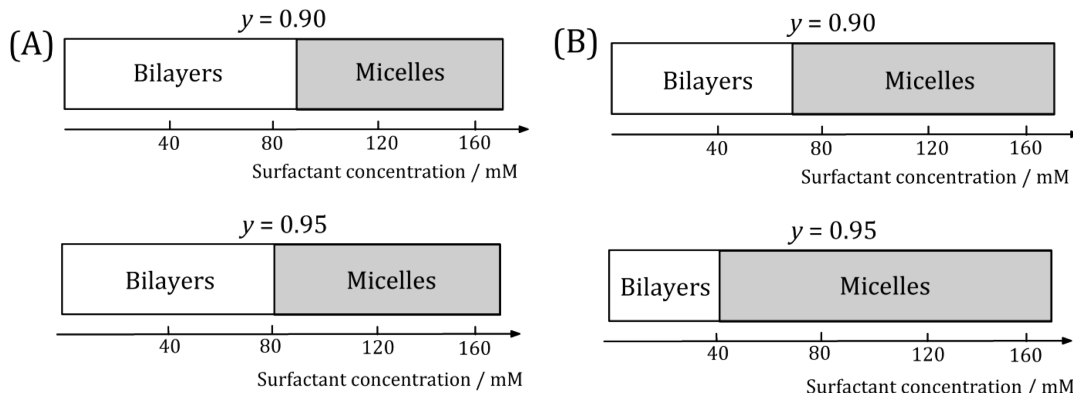


Figure 8. Diagrams showing surfactant concentrations and compositions where either micelles or bilayer aggregates predominate according to (A) SANS and SLS and (B) cryo-TEM.

able to safely conclude that the SANS and SLS to all intents and purposes give more or less identical results, and that the choice of either H₂O or D₂O as solvent does not significantly influence the structural behavior in SOS-rich mixtures of SOS and CTAB.

However, the agreement between cryo-TEM, on the one hand, and the two scattering techniques, on the other hand, is less obvious. Figure 8 shows predominance diagrams indicating at which surfactant concentrations and compositions either micelles or bilayer aggregates predominate according to either SANS and SLS (Figure 8A) or cryo-TEM (Figure 8B), and it is seen that micelles appear to predominate in a much wider regime according to cryo-TEM. The diagrams are based on the results given in Table 1 (SANS) and Tables 4 and 5 (cryo-TEM and SLS), respectively. In accordance, an abrupt transition from micelles to bilayers occurs at [$y = 0.95, 80\text{ mM}$] according to SANS where micelles and bilayers are observed to coexist, whereas both micelles and bilayers may be seen in cryo-TEM images for the sample [$y = 0.95, 40\text{ mM}$]. For the series $y = 0.90$, only micelles are observed with SANS at 100 mM, whereas only bilayers are observed at 80 mM, and we have roughly set the point of transition to 90 mM. Similarly, the point of transition according to cryo-TEM roughly appears at 70 mM at $y = 0.90$.

A good agreement between all experimental techniques is observed for the most diluted samples at surfactant

compositions $y = 0.90$ [cf., Figure 8 and Table 5]. Examples of two cryo-TEM images for the sample [$y = 0.90, 20\text{ mM}$] are shown in Figure 9A,B, and the SANS data for the same sample are shown in Figure 9C. The sample contains, according to SANS, 72% vesicles coexisting with 28% disks. Several cryo-TEM images show the presence of polydisperse unilamellar vesicles but also vesicles breaking up to form open bilayers [cf., Figure 9A]. Other images for the very same sample, but at a different location on the grid, show only perfect unilamellar vesicles [cf., Figure 9B]. The vesicle size observed with cryo-TEM is in qualitative agreement with what we have determined by SANS, that is, $R_v \approx 28\text{--}42\text{ nm}$ [cf., Table 1].

From a small-angle scattering point of view, it is difficult to distinguish between flat disks and substantially open vesicles as seen in Figure 9A, and our SANS data could always be excellently fitted with a model for coexisting vesicles and disks. It is possible that Figure 8A captures a dynamic process where geometrically closed vesicles are bursting and opening to form disklike aggregates. This view is supported by the fact that open vesicles are always observed together with closed vesicles, and that only closed vesicles are frequently observed at certain positions on the very same liquid film investigated with cryo-TEM. Notably, the transformation from geometrically closed vesicles to open vesicles or disks corresponds to a change in topology of the bilayer aggregates.⁵⁸

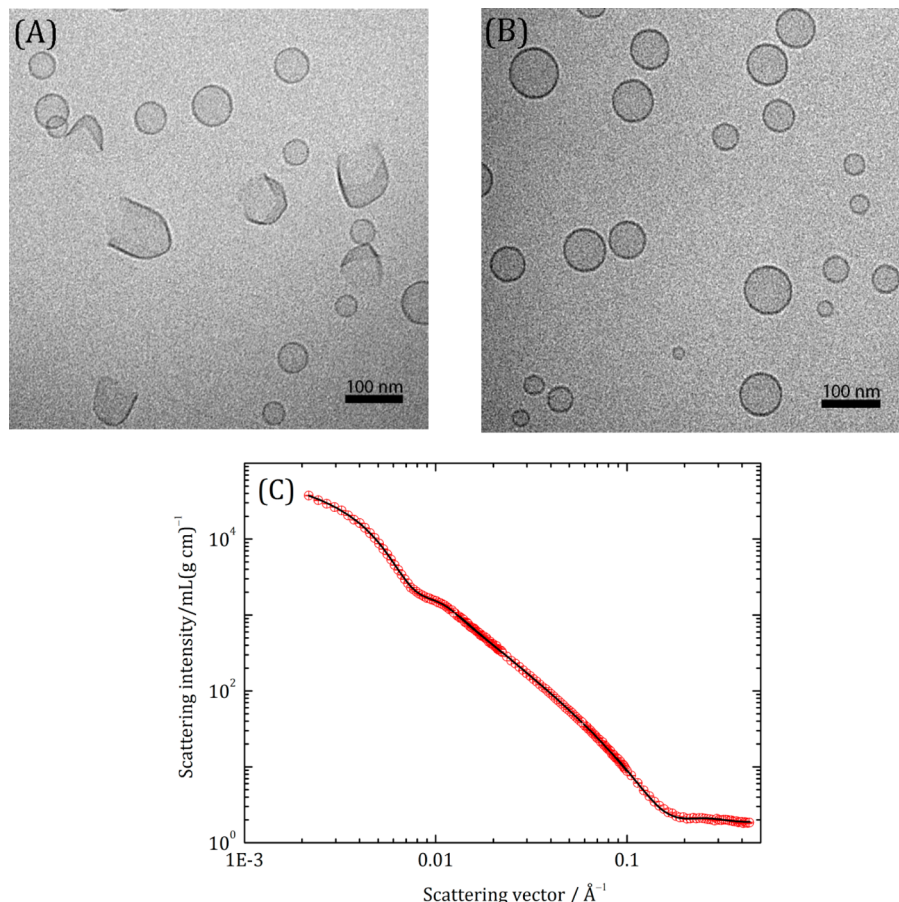


Figure 9. (A,B) Cryo-TEM images for the sample $y \equiv [\text{SOS}]/([\text{SOS}] + [\text{CTAB}]) = 0.90$ and overall surfactant concentration $[\text{SOS}] + [\text{CTAB}] = 20 \text{ mM}$ at two different locations on the grid. (C) Normalized scattering cross section as a function of the scattering vector q for the same sample (○). Symbols represent SANS data obtained for different sample-detector distances. The solid line represents the best available fit with a model for coexisting bilayer vesicles (72%) and disks (28%). Results from the least-squares model fitting analysis are given in Table 1. The quality of the fit as measured by the reduced chi-squared parameter χ^2 is 4.0.

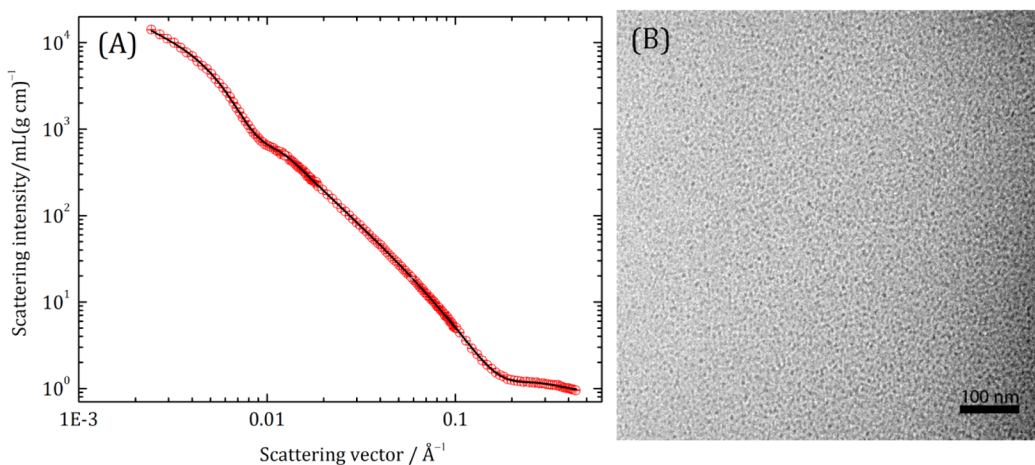


Figure 10. (A) Normalized scattering cross section as a function of the scattering vector q for mixtures of SOS and CTAB in deuterium oxide in the absence of added salt for a given mole fraction of SOS in solution $y \equiv [\text{SOS}]/([\text{SOS}] + [\text{CTAB}]) = 0.95$ and an overall surfactant concentration of the samples $[\text{SOS}] + [\text{CTAB}] = 60 \text{ mM}$ (○). Symbols represent SANS data obtained for different sample-detector distances. The solid line represents the best available fit with a model for coexisting bilayer vesicles (49%) and disks (51%). Results from the least-squares model fitting analysis are given in Table 1. The quality of the fit as measured by χ^2 is 3.2. (B) Typical cryo-TEM image for the same sample [$y = 0.95, 60 \text{ mM}$] in water or deuterium oxide. Only apparently globular micelles and no bilayer structures are observed.

Mixtures of SOS and CTAB in the absence of added salt have previously been investigated with cryo-TEM by Yatilla et al.¹⁰ The results as to the structure of bilayers formed in the SOS-

rich regime seem to differ somewhat between the study reported in ref 10 and our present cryo-TEM measurements. Bilayer disks or vesicles that open as seen in Figure 9A were

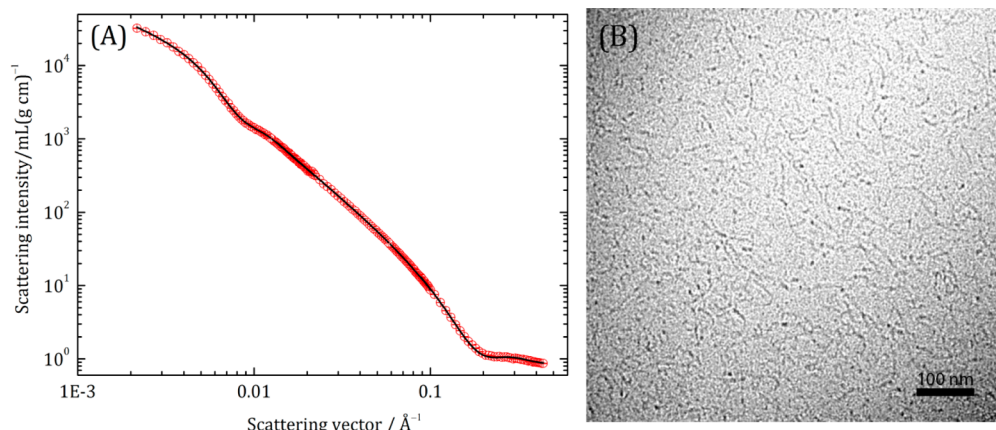


Figure 11. (A) Normalized scattering cross section as a function of the scattering vector q for mixtures of SOS and CTAB in deuterium oxide in the absence of added salt for a given mole fraction of SOS in solution $y \equiv [\text{SOS}]/([\text{SOS}] + [\text{CTAB}]) = 0.90$ and an overall surfactant concentration of the samples $[\text{SOS}] + [\text{CTAB}] = 80 \text{ mM}$ (\circ). Symbols represent SANS data obtained for different sample-detector distances. The solid line represents the best available fit with a model for coexisting bilayer vesicles (59%) and disks (41%). Results from the least-squares model fitting analysis are given in Table 1. The quality of the fit as measured by χ^2 is 5.8. (B) Typical cryo-TEM image for the same sample [$y = 0.90, 80 \text{ mM}$]. Only wormlike micelles and no bilayer structures are observed.

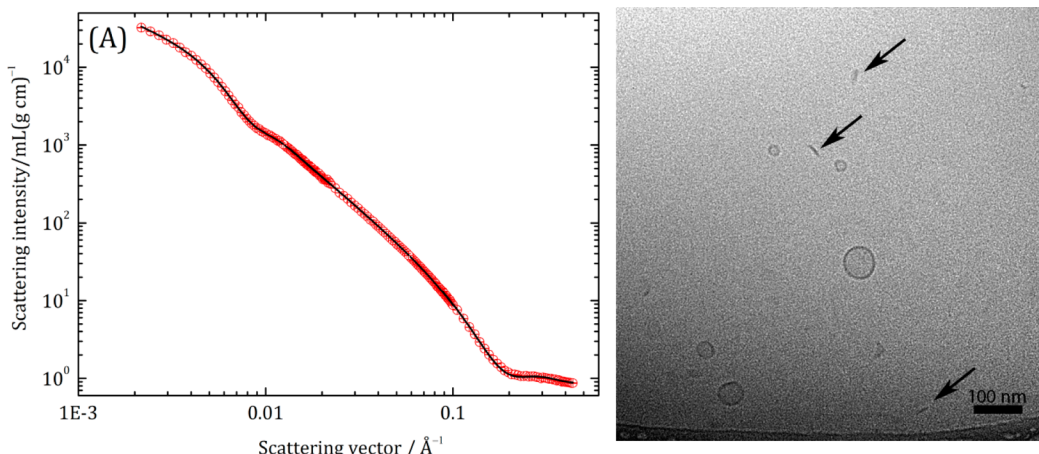


Figure 12. (A) Normalized scattering cross section as a function of the scattering vector q for mixtures of SOS and CTAB in deuterium oxide in the absence of added salt for a given mole fraction of SOS in solution $y \equiv [\text{SOS}]/([\text{SOS}] + [\text{CTAB}]) = 0.95$ and an overall surfactant concentration of the samples $[\text{SOS}] + [\text{CTAB}] = 40 \text{ mM}$ (\circ). Symbols represent SANS data obtained for different sample-detector distances. The solid line represents the best available fit with a model for coexisting bilayer vesicles (56%) and disks (44%). Results from the least-squares model fitting analysis are given in Table 1. The quality of the fit as measured by χ^2 is 3.0. (B) Cryo-TEM image for the same sample [$y = 0.95, 40 \text{ mM}$] in deuterium oxide showing vesicles and disks. The arrows indicate disks observed edge-on. Other images for the very same sample show only slightly elongated micelles but no bilayer aggregates.

never reported in ref 10. On the other hand, it was emphasized that SOS-rich vesicles were evidently nonspherical and sometimes tubular in shape. This is in contrast with our present observations according to which the vesicles are always fairly spherical in shape in the absence of added salt [cf., Figure 9B].

Most surprisingly, as shown in Figure 8 and Tables 4 and 5, there is an obvious discrepancy between the outcomes of cryo-TEM, on the one hand, and both scattering techniques, SANS and SLS, on the other hand, for some of our samples. For instance, Figure 10B shows a typical cryo-TEM image for the sample [$y = 0.95, 60 \text{ mM}$], that is, a sample with a concentration well within the regime where bilayers are observed with SANS [cf., Figure 10A] and SLS. Contrary to the expectations, only small compact globular micelles are observed in the cryo-TEM images. The appearance of these micelles agrees very well with the small spheroidal or ellipsoidal

micelles observed with SLS and SANS at higher surfactant concentrations, that is, micelles considerably shorter than 10 nm. Neither vesicles nor any other bilayer structures could be observed in any of the micrographs from this sample, despite the fact that the sample had a bluish appearance to the bare eye, indicating the presence of vesicles.

In fact, several of our samples show a similar discrepancy between cryo-TEM, on the one hand, and SANS and SLS, on the other. The discrepancy tends to show up in samples close to the micelle-to-bilayer transition, for instance, at [$y = 0.95, 40$, and 60 mM] and [$y = 0.90, 80 \text{ mM}$]. Long rodlike micelles are present in a rather narrow regime according to SANS and are observed in only three samples: [$y = 0.90, 100$, and 120 mM] and [$y = 0.95, 100 \text{ mM}$]. Nevertheless, moderately long flexible wormlike micelles are captured with cryo-TEM in the sample [$y = 0.90, 80 \text{ mM}$] [cf., Figure 11B]. The wormlike micelles seen in Figure 11B appear to be a few hundreds of Angstroms long in

qualitative agreement with the average length determined with SANS for the micelles in the sample [$y = 0.90, 100 \text{ mM}$]. However, only bilayers are present in the sample [$y = 0.90, 80 \text{ mM}$] according to SANS and SLS [cf., Figure 11A].

Two of the samples that show different results depending on experimental techniques were also measured with cryo-TEM using D_2O instead of H_2O as solvent. In accordance, we find that the discrepancy between cryo-TEM and SANS appears irrespective of solvent that is chosen. No difference at all could be seen with cryo-TEM for the sample [$y = 0.95, 60 \text{ mM}$] depending on whether H_2O or D_2O was used as solvent, and only small globular micelles were always observed. For the sample [$y = 0.95, 40 \text{ mM}$], however, we observe a difference with cryo-TEM in D_2O as compared to H_2O . In the former case, either slightly elongated micelles or (closed and open) vesicles, and sometimes disks, could be seen depending on the position on the grid [cf., Figure 12B], whereas only small micelles were seen in the corresponding sample with H_2O as solvent. Probably, this sample is located very close to the micelle-to-bilayer transition as seen with cryo-TEM [cf., Figure 8B]. The disks observed in one of the images for the sample [$y = 0.95, 40 \text{ mM}$] appear to be about a factor of 2 or 3 smaller as compared to the average value determined with SANS [cf., Figure 12B].

In summary, we may conclude that all aggregate types observed with SANS and SLS, that is, small compact micelles, large elongated micelles, and coexisting closed and open bilayers, are also observed with cryo-TEM, but not necessarily at the same surfactant concentrations. For the samples where a discrepancy between microscopy and scattering techniques occurs, the cryo-TEM images always show the presence of small compact or somewhat bigger wormlike micelles, whereas bilayer structures (vesicles and disks), and no micelles, are present in the samples according to SANS and SLS.

As a matter of fact, a similar difference between cryo-TEM and dynamic light scattering has previously been reported for SOS-rich mixtures of SOS and CTAB by Yatcilla et al.,¹⁰ and the discrepancy between the different techniques appears to be unusually evident in this particular system. It was suggested in ref 10 that vesicles contribute to the scattering behavior and the bluish appearance of the samples but are too few, due to coexistence with micelles, to be observed with cryo-TEM. This explanation is, however, not consistent with our present SANS results, according to which no micelles at all are present in the corresponding samples. It is also concluded from our SANS study that micelles and vesicles coexist in a much more narrow regime of surfactant concentrations and compositions than what corresponds to the regimes of discrepancy shown in Figure 8. Moreover, the difference between SANS/SLS and cryo-TEM always appears in a consistent manner in that micelles are observed with cryo-TEM, whereas bilayers are present according to the scattering techniques.

We propose a different explanation to this phenomenon and suggest that the equilibrium situation in a system with comparatively fast dynamics may be significantly distorted during the process of sample preparation in connection with the cryo-TEM measurements. In accordance, rearrangements in distribution of the two surfactants may begin to occur at the moment the droplet to be measured is introduced to grid and affect the structural properties of bulk aggregates. In particular, this equilibrium situation is expected to be influenced by the fact that, in the sample preparation process of cryo-TEM, a concave lens-like film as thin as about 10–500 nm is created.⁴³

Surfactants are surface active components and tend to enrich at interfaces. Usually the amount of surfactant adsorbed at interfaces is negligible. However, the interfacial area present in the thin cryo-TEM film must be unusually large in relation to the film bulk volume.

For instance, an area per surfactant molecule at the air–water interface equal to about 40 \AA^2 , that is, a typical value for a surfactant with a sulfate headgroup,⁵⁹ corresponds to a surface concentration of adsorbed surfactant of about $4 \times 10^{-9} \text{ mol m}^{-2}$. Comparison with the corresponding concentration of surfactant in bulk at $c_t = 80 \text{ mM}$, obtained by multiplying c_t by the film thickness <500 nm, gives $4 \times 10^{-8} \text{ mol m}^{-2}$ and more than 10% of the surfactant adsorbed at interfaces. This value is expected to increase as the samples are further diluted.

This means that the amount of surfactant incorporated in bulk aggregates is expected to be of comparable magnitude to the amount of surfactant at interfaces, which may influence the distribution of the two surfactants SOS and CTAB among bulk aggregates and monolayers at interfaces. Intuitively, one might expect that the presence of the air/water interfaces should bring about the same effect as that of simply diluting the solution. This requires, however, that the surfactant monolayers adsorbed at the interfaces have a composition that is similar to that in the bulk solution. For electrostatic and curvature reasons, it is more likely, however, that the surfactant monolayers at the planar (i.e., with mean curvature equal to zero) interfaces have a composition comparable to that found in SOS/CTAB bilayers. As a consequence, the bulk aggregates observed in the thin film investigated with cryo-TEM may become enriched with SOS, generating micelles rather than the bilayers observed in the in situ measurements using scattering techniques.

Notably, the discrepancy between the different techniques appears to be more pronounced for the dilution series $y = 0.95$ than for the series $y = 0.90$ [cf., Figure 8]. This may be due to the circumstance that, because of the presence of a considerable amount of free surfactant, the concentration of bulk aggregates is significantly lower in samples at $y = 0.95$, as compared to samples at $y = 0.90$, at identical values of $[\text{SOS}] + [\text{CTAB}]$ [cf., calculated values tabulated in the Supporting Information].

CONCLUSIONS

The structural behaviors of self-assembled aggregates in the dilute regimes of SOS-rich mixtures of the anionic surfactant SOS and the cationic surfactant CTAB have been investigated by means of comparing results from the complementary techniques small-angle neutron scattering (SANS), static light scattering (SLS), and cryo-transmission electron microscopy (cryo-TEM). Because of the high critical micelle concentration of SOS, a large amount of free surfactant is always present in our samples coexisting with the self-assembled aggregates. As a matter of fact, the mass fraction of free surfactant is always larger than the fraction of aggregates in the samples investigated in this work. The results from our model calculations based on the Poisson–Boltzmann theory are confirmed by SANS data analysis, according to which the presence of free surfactant contributes significantly to the scattering behavior in the regime of high scattering vector moduli.

By means of combining theoretical calculations with detailed experimental investigations, we have been able to, for the first time, rationalize in a quantitative manner the dramatic changes in microstructure, from small spheroidal micelles to large bilayer aggregates, that is frequently observed upon simply

diluting mixtures of an anionic and a cationic surfactant. As a consequence of the fact that the fraction of surfactant present as free monomers increases upon diluting a surfactant mixture, the composition in the self-assembled bulk aggregates must be a function of total surfactant concentration. As a result, we observe a growth of small oblate spheroidal or general ellipsoidal micelles to long rodlike or wormlike micelles as the mole fraction of SOS in the micelles (x), and the surface charge density, decreases. At about $x = 0.70$, an abrupt transition from micelles to bilayers is observed, and x approaches a value close to equimolarity ($x = 0.5$) as the samples are further diluted. From the SANS measurements, we are able to conclude that samples with bilayers consist of coexisting vesicles and disks.

All different aggregate types observed with SANS and SLS, that is, small compact micelles, large rodlike micelles, and coexisting bilayer vesicles and disks, are also observed with cryo-TEM, but not necessarily in identical samples. In other words, while SANS (samples with D_2O as solvent) and SLS (samples with H_2O as solvent) always agree with respect to whether small micelles, large micelles, or bilayers are present in the samples, we do in several cases observe a conspicuous discrepancy between SANS/SLS, on the one hand, and cryo-TEM, on the other hand. More specifically, only small globular or somewhat larger wormlike micelles can be observed with cryo-TEM in some of our samples in the vicinity of the micelle-to-bilayer transition, although the samples appear bluish to the bare eye, and only bilayer structures (vesicles and disks), and no micelles, are present according to the scattering data.

A similar discrepancy between cryo-TEM and dynamic light scattering regarding whether micelles or bilayers are present in a particular sample has previously been observed, and it was suggested to be a consequence of coexistence between micelles and bilayers.¹⁰ However, our present results are inconsistent with this explanation. Instead, we suggest that the presence of an unusually high free surfactant concentration, giving rise to fast dynamic processes in the SOS-CTAB system, together with the high fraction of surfactant adsorbed at the interfaces of the thin film of sample created during the cryo-TEM measurements, exert an influence on the results from the microscopy technique. Because the surfactant monolayers at interfaces have a planar geometry, with a mean curvature equal to zero, the presence of a non-negligible amount of adsorbed surfactant tends to change the composition in the bulk aggregates in such a way that substantially curved micelles become more favored close to the micelle-to-bilayer transition.

Our discovery that discrepancies between *in situ* scattering and *ex situ* microscopy techniques may exist in certain surfactant systems, together with our novel interpretation of this phenomenon, is expected to have an important impact on future experimental studies of different systems in which surfactants are present. Hence, we may conclude that cryo-TEM gives a direct image of the different aggregate types that may form in a particular system, but not necessarily in the particular sample investigated. SANS, on the other hand, is a more suitable technique to quantitatively follow structural changes and transformations of self-assembled aggregates in response to, for instance, surfactant concentration, composition, and electrolyte concentration.

ASSOCIATED CONTENT

S Supporting Information

Models employed in the least-square fitting data analysis. Comparison of model fits with or without structure factor for ellipsoidal micelles. Calculations of the surfactant mole fraction in micelles. This material is available free of charge via the Internet at <http://pubs.acs.org>.

AUTHOR INFORMATION

Corresponding Author

*Tel.: +46 8 790 99 21. Fax: +46 8 20 82 84. E-mail: magnusbe@kth.se.

Notes

The authors declare no competing financial interest.

ACKNOWLEDGMENTS

Institut Laue Langevin (ILL) is acknowledged for allocated SANS beam time (proposal 9-10-1181). K.E. was supported by the Swedish Research Council (VR).

APPENDIX A: LIST OF SYMBOLS OF PARAMETERS PRESENT IN TABLES 1 AND 2

a	half axis related to thickness of ellipsoidal micelles
b	half axis related to width of ellipsoidal micelles
c	half axis related to length of ellipsoidal micelles
c_{el}	electrolyte concentration
c_{mic}	concentration of surfactant aggregated in micelles
f_d	mass fraction of bilayer disks coexisting with bilayer vesicles
f_m	mass fraction of micelles coexisting with bilayer disks and vesicles
f_v	mass fraction of bilayer vesicles coexisting with bilayer disks
$\langle L \rangle$	volume-averaged length of polydisperse rod-like micelles
l_s	length of free surfactant monomer
$N, N', \langle N \rangle, N_{SLS}$	aggregation number of micelles
R_d	disk radius
R_v	volume-averaged vesicle radius
r_c	radius of cylindrical micelle
z_{eff}	effective charge of micelle
z_{id}	charge of micelle with fully dissociated surfactants
$\alpha = z_{eff}/z_{id}$	relative effective charge of micelle
ξ	thickness of self-assembled monolayer in bilayer disks and vesicles (half bilayer thickness)
$\sigma_L/\langle L \rangle$	relative standard deviation with respect to length of polydisperse rodlike micelles
σ_v/R_v	relative standard deviation with respect to radius of polydisperse vesicles

REFERENCES

- (1) Edwards, K.; Almgren, M.; Bellare, J.; Brown, W. Effects of Triton X-100 on sonicated lecithin vesicles. *Langmuir* 1989, 5, 473–478.
- (2) Vinson, P. K.; Talmon, Y.; Walter, A. Vesicle-micelle transition of phosphatidylcholine and octyl glucoside elucidated by cryo-transmission electron microscopy. *Biophys. J.* 1989, 56, 669–681.

- (3) Egelhaaf, S. U.; Schurtenberger, P. Shape transformations in the Lecithin-bile salt system: From cylinders to vesicles. *J. Phys. Chem.* **1994**, *98*, 8560–8573.
- (4) Aratono, M.; Onimaru, N.; Yoshikai, Y.; Shigehisa, M.; Koga, I.; Wongwailikit, K.; Ohta, A.; Takiue, T.; Lhoussaine, B.; Strey, R.; Takata, Y.; Villeneuve, M.; Matsubara, H. Spontaneous vesicle formation of single chain and double chain cationic surfactant mixtures. *J. Phys. Chem. B* **2007**, *111*, 107–115.
- (5) Grillo, I.; Penfold, J.; Tucker, I.; Cousin, F. Spontaneous formation of nanovesicles in mixtures of nonionic and dialkyl chain cationic surfactants studied by surface tension and SANS. *Langmuir* **2009**, *25*, 3932–3943.
- (6) Grillo, I.; Penfold, J. Self-assembly of mixed anionic and nonionic surfactants in aqueous solution. *Langmuir* **2011**, *27*, 7453–7463.
- (7) Bergström, L. M.; Skoglund, S.; Danerlöv, K.; Garamus, V. M.; Pedersen, J. S. The growth of micelles, and the transition to bilayers, in mixtures of a single-chain and a double-chain cationic surfactant investigated with small-angle neutron scattering. *Soft Matter* **2011**, *7*, 10935–10944.
- (8) Kaler, E. W.; Murthy, A. K.; Rodriguez, B. E.; Zasadzinski, J. A. N. Spontaneous vesicle formation in aqueous mixtures of single-tailed surfactants. *Science* **1989**, *245*, 1371–1374.
- (9) Kaler, E. W.; Herrington, K. L.; Murthy, A. K.; Zasadzinski, J. A. N. Phase behavior and structures of mixtures of anionic and cationic surfactants. *J. Phys. Chem.* **1992**, *96*, 6698–6707.
- (10) Yatcilla, M. T.; Herrington, K. L.; Brasher, L. L.; Kaler, E. W.; Chiruvolu, S.; Zasadzinski, J. A. N. Phase behavior of aqueous mixtures of cetyltrimethylammonium bromide (CTAB) and sodium octyl sulfate (SOS). *J. Phys. Chem.* **1996**, *100*, 5874–5879.
- (11) Bergström, M.; Pedersen, J. S. A small-angle neutron scattering (SANS) study of tablet-shaped and ribbonlike micelles formed from mixtures of an anionic and a cationic surfactant. *J. Phys. Chem. B* **1999**, *103*, 8502–8513.
- (12) Bergström, M.; Pedersen, J. S.; Schurtenberger, P.; Egelhaaf, S. U. Small-angle neutron scattering (SANS) study of vesicles and lamellar sheets formed from mixtures of an anionic and a cationic surfactant. *J. Phys. Chem. B* **1999**, *103*, 9888–9897.
- (13) Herrington, K. L.; Kaler, E. W.; Miller, D. D.; Zasadzinski, J. A. N.; Chiruvolu, S. Phase behavior of aqueous mixtures of dodecyltrimethylammonium bromide (DTAB) and sodium dodecyl sulfate (SDS). *Langmuir* **1993**, *97*, 13792–13802.
- (14) Chiruvolu, S.; Israelachvili, J. N.; Naranjo, E.; Xu, Z.; Zasadzinski, J. A.; Kaler, E.; Herrington, K. L. Measurement of forces between spontaneous vesicle-forming bilayers. *Langmuir* **1995**, *11*, 4256–4266.
- (15) Yaacob, I. I.; Bose, A. An investigation of microstructures in cationic/anionic surfactant suspensions by cryogenic transmission electron microscopy. *J. Colloid Interface Sci.* **1996**, *178*, 638–647.
- (16) Brasher, L. L.; Kaler, E. W. A Small-angle neutron scattering (SANS) contrast variation investigation of aggregate composition in catanionic surfactant mixtures. *Langmuir* **1996**, *12*, 6270–6276.
- (17) Zana, R.; Levy, H.; Danino, D.; Talmon, Y.; Kwtetkat, K. Mixed micellization of cetyltrimethylammonium bromide and an anionic dimeric (Gemini) surfactant in aqueous solution. *Langmuir* **1997**, *13*, 402–408.
- (18) Marques, E. F.; Regev, O.; Khan, A.; da Graça Miguel, M.; Lindman, B. Vesicle formation and general phase behavior in the catanionic mixture SDS-DDAB-water. The cationic-rich side. *J. Phys. Chem. B* **1999**, *103*, 8353–8363.
- (19) Villeneuve, M.; Kaneshina, S.; Imae, T.; Aratono, M. Vesicle-micelle equilibrium of anionic and cationic surfactant mixture studied by surface tension. *Langmuir* **1999**, *15*, 2029–2036.
- (20) Tondre, C.; Caillet, C. Properties of the amphiphilic films in mixed cationic/anionic vesicles: a comprehensive view from a literature analysis. *Adv. Colloid Interface Sci.* **2001**, *93*, 115–134.
- (21) Prévost, S.; Wattebled, L.; Laschewsky, A.; Gradzielski, M. Formation of monodisperse charged vesicles in mixtures of cationic Gemini surfactants and anionic SDS. *Langmuir* **2011**, *27*, 582–591.
- (22) Tian, M.; Zhu, L.; Yu, D.; Wang, Y.; Sun, S.; Wang, Y. Aggregate transitions in mixtures of anionic sulfonate Gemini surfactant with cationic ammonium single-chain surfactant. *J. Phys. Chem. B* **2013**, *117*, 443–440.
- (23) Marques, E. F.; Regev, O.; Khan, A.; da Graça Miguel, M.; Lindman, B. Vesicle formation and general phase behavior in the catanionic mixture SDS-DDAB-water. The anionic-rich side. *J. Phys. Chem. B* **1998**, *102*, 6746–6758.
- (24) Hao, J.; Hoffmann, H. Self-assembled structures in excess and salt-free catanionic surfactant solutions. *Curr. Opin. Colloid Interface Sci.* **2004**, *9*, 279–293.
- (25) Söderman, O.; Herrington, K. L.; Kaler, E. W.; Miller, D. D. Transition from micelles to vesicles in aqueous mixtures of anionic and cationic surfactants. *Langmuir* **1997**, *13*, 5531–5538.
- (26) Bergström, L. M.; Aratono, M. Synergistic effects in mixtures of two identically charged ionic surfactants with different critical micelle concentrations: A comparison between theoretical predictions and experimental observations. *Soft Matter* **2011**, *7*, 8870–8879.
- (27) Bergström, M.; Pedersen, J. S. A small-angle neutron scattering study of surfactant aggregates formed in aqueous mixtures of sodium dodecyl sulfate and didodecyldimethylammonium bromide. *J. Phys. Chem. B* **2000**, *104*, 4155–4163.
- (28) Cotton, J. P. Introduction to scattering experiments. In *Neutron, X-Ray and Light Scattering: Introduction to an Investigative Tool for Colloidal and Polymeric Systems*; Lindner, P., Zemb, T., Eds.; North-Holland: Amsterdam, 1991; pp 3–18.
- (29) Cotton, J. P. Initial data treatment. In *Neutron, X-Ray and Light Scattering: Introduction to an Investigative Tool For Colloidal and Polymeric Systems*; Lindner, P., Zemb, T., Eds.; North-Holland: Amsterdam, 1991; pp 19–31.
- (30) Hayter, J. B.; Penfold, J. An analytic structure factor for macroion solutions. *Mol. Phys.* **1981**, *42*, 109–118.
- (31) Hansen, J. P.; Hayter, J. B. A rescaled MSA structure factor for dilute charged colloidal dispersions. *Mol. Phys.* **1982**, *46*, 651–656.
- (32) Kotlarchyk, M.; Chen, S. H. Analysis of small angle neutron scattering spectra from polydisperse interacting colloids. *J. Chem. Phys.* **1983**, *79*, 2461–2469.
- (33) Hayter, J. B.; Penfold, J. Determination of micelle structure and charge by neutron small-angle scattering. *Colloid Polym. Sci.* **1983**, *261*, 1027–1030.
- (34) Pedersen, J. S. Analysis of small-angle scattering data from colloids and polymer solutions: Modeling and least-squares fitting. *Adv. Colloid Interface Sci.* **1997**, *70*, 171–210.
- (35) Tanford, C. *The Hydrophobic Effect*; Wiley: New York, 1980.
- (36) Chevalier, Y.; Zemb, T. The structure of micelles and microemulsions. *Rep. Prog. Phys.* **1990**, *53*, 279–371.
- (37) Corkill, J. M.; Goodman, J. M.; Walker, T. Partial molar volumes of surface-active agents in aqueous solution. *Trans. Faraday Soc.* **1967**, *63*, 768–772.
- (38) Pedersen, J. S. Resolution effects and analysis of small-angle neutron scattering data. *J. Phys. IV (Paris)* **1993**, *3*, 491–498.
- (39) Pedersen, J. S.; Posselt, D.; Mortensen, K. Analytical treatment of the resolution function for small-angle scattering. *J. Appl. Crystallogr.* **1990**, *23*, 321–333.
- (40) Bevington, B. R. *Data Reduction and Error Analysis for Physical Sciences*; McGraw-Hill: New York, 1969.
- (41) Coumou, D. J.; Mackor, E. L.; Humans, J. Isotropic light-scattering in pure liquids. *Trans. Faraday Soc.* **1964**, *60*, 1539–1547.
- (42) Kaye, W.; McDaniel, J. B. Low-angle laser light scattering-Rayleigh factors and depolarization ratios. *Appl. Opt.* **1974**, *13*, 1936–1937.
- (43) Almgren, M.; Edwards, K.; Karlsson, G. Cryo transmission electron microscopy of liposomes and related structures. *Colloids Surf. A* **2000**, *174*, 3–21.
- (44) Bergström, L. M.; Bramer, T. Synergistic effects in mixtures of oppositely charged surfactants as calculated from the Poisson–Boltzmann theory: A comparison between theoretical predictions and experiments. *J. Colloid Interface Sci.* **2008**, *322*, 589–595.

- (45) Kamenka, N.; Chorro, M.; Talmon, Y.; Zana, R. Study of mixed aggregates in aqueous solutions of sodium dodecyl sulfate and dodecyltrimethylammonium bromide. *Colloids Surf.* **1992**, *67*, 213–222.
- (46) Haydon, D. A.; Taylor, F. H. Adsorption of sodium octyl and decyl sulphates and octyl and decyl trimethylammonium bromides at the decane-water interface. *Trans. Faraday Soc.* **1962**, *58*, 1233–1250.
- (47) Huisman, H. F. Light scattering of solutions of ionic detergents. III. *Proc. K. Ned. Akad. Wet., Ser. B* **1964**, *67*, 388–406.
- (48) Czerniawski, M. The double layer structure of colloidal electrolytes. III. Electrolytic conductivity of aqueous cetyltrimethylammonium bromide solutions. *Roczn. Chem.* **1966**, *40*, 1935–1945.
- (49) Imae, T.; Kamiya, R.; Ikeda, S. Formation of spherical and rodlike micelles of cetyltrimethylammonium bromide in aqueous NaBr solutions. *J. Colloid Interface Sci.* **1985**, *108*, 215–225.
- (50) Israelachvili, J. N. *Intermolecular and Surface Forces*, 3rd ed.; Academic Press: New York, 2011.
- (51) Bergström, L. M. Thermodynamics of self-assembly. In *Application of Thermodynamics to Biological and Material Science*; Tadashi, M., Ed.; InTech: Rijeka, 2011; Vol. 11, pp 289–314.
- (52) Bergström, M.; Pedersen, J. S. Formation of tablet-shaped and ribbonlike micelles in mixtures of an anionic and a cationic surfactant. *Langmuir* **1999**, *15*, 2250–2253.
- (53) Bergström, L. M.; Garamus, V. M. Structural behaviour of mixed cationic surfactant micelles: A small-angle neutron scattering study. *J. Colloid Interface Sci.* **2012**, *381*, 89–99.
- (54) Bergström, M.; Kjellin, U. R. M.; Claesson, P. M.; Grillo, I. A small-angle neutron scattering study of mixtures of cationic polyelectrolyte and anionic surfactant: Effect of polyelectrolyte charge density. *J. Phys. Chem. B* **2004**, *108*, 1874–1881.
- (55) Jerke, G.; Pedersen, J. S.; Egelhaaf, S. U.; Schurtenberger, P. Static structure factor of polymerlike micelles: Overall dimension, flexibility, and local properties of lecithin reverse Mmicelles in deuterated isoctane. *Phys. Rev. E* **1997**, *56*, 5772–5788.
- (56) Bergström, L. M. Model calculations of the spontaneous curvature, mean and Gaussian bending constants for a thermodynamically open surfactant film. *J. Colloid Interface Sci.* **2006**, *293*, 181–193.
- (57) Bergström, L. M. Bending energetics of tablet-shaped micelles: A novel approach to rationalize micellar systems. *ChemPhysChem* **2007**, *8*, 462–472.
- (58) Hyde, S.; Andersson, S.; Larsson, K.; Blum, Z.; Landh, T.; Lidin, S.; Ninham, B. W. *The Language of Shape*; Elsevier: Amsterdam, 1997.
- (59) Jönsson, B.; Lindman, B.; Holmberg, K.; Kronberg, B. *Surfactant and Polymers in Aqueous Solution*; Wiley: Chichester, 1998.